ACS Sustainable Chemistry & Engineering

Article

Valorization of acid isolated high yield lignin nanoparticles as innovative antioxidant/antimicrobial organic materials

Weijun Yang, Elena Fortunati, Daqian Gao, Giorgio Mariano Balestra, Geremia Giovanale, Xiaoyan He, Luigi Torre, Josè M. Kenny, and Debora Puglia

ACS Sustainable Chem. Eng., **Just Accepted Manuscript** • DOI: 10.1021/acssuschemeng.7b03782 • Publication Date (Web): 11 Jan 2018

ACS Publications

ACS Sustainable Chemistry & Engineering is published by the American Chemical Society. 1155 Sixteenth Street N.W., Washington, DC 20036

Valorization of acid isolated high yield lignin nanoparticles as innovative antioxidant/antimicrobial organic materials

Weijun Yang, Elena Fortunati, Daqian Gao, Giorgio M. Balestra, G. Giovanale, Xiaoyan He, Luigi Torre, José M. Kenny, Debora Puglia

Weijun Yang, *University of Perugia, Civil and Environmental Engineering Department, Materials Engineering Center, UdR INSTM, Strada di Pentima 4, 05100, Terni, Italy,* weijun.yang2012@gmail.com

Elena Fortunati, *University of Perugia, Civil and Environmental Engineering Department, Materials Engineering Center, UdR INSTM, Strada di Pentima 4, 05100, Terni, Italy,* elena.fortunati@unipg.it

Daqian Gao, *Changchun Institute of Applied Chemistry, Chinese Academy of Sciences, CIAS, CAS, Renmin Road 5625, 130022, Changchun, P.R. China, gaodaqiannefu@ciac.ac.cn*

Giorgio M. Balestra, *University of Tuscia, Department of Agricultural Science and Forestry (DAFNE), Via S. Camillo De Lellis snc, 01100 Viterbo, Italy, balestra@unitus.it*

Geremia Giovanale, *University of Tuscia, Department of Agricultural Science and Forestry (DAFNE), Via S. Camillo De Lellis snc, 01100 Viterbo, Italy, geremiagiovanale@gmail.com*

Xiaoyan He, *Northeast Forestry University, Materials Science and Engineering School, Hexing Road 26, 150040, Harbin, P.R. China, University of Perugia, Civil and Environmental Engineering Department, Materials Engineering Center, UdR INSTM, Strada di Pentima 4, 05100, Terni, Italy*, pghxy@hotmail.com

Luigi Torre, *University of Perugia, Civil and Environmental Engineering Department, Materials Engineering Center, UdR INSTM, Strada di Pentima 4, 05100, Terni, Italy, luigi.torre@unipg.it*

José M. Kenny, *University of Perugia, Civil and Environmental Engineering Department, Materials Engineering Center, UdR INSTM, Strada di Pentima 4, 05100, Terni, Italy*, jose.kenny@unipg.it

Debora Puglia, *University of Perugia, Civil and Environmental Engineering Department, Materials Engineering Center, UdR INSTM, Strada di Pentima 4, 05100, Terni, Italy,* debora.puglia@unipg.it

**Corresponding author: debora.puglia@unipg.it; Tel +390744492916; Fax +390744492950*

Abstract

In this study, dissolution of pristine alkali lignin into ethylene glycol, followed by addition of different acidic conditions (HCl, H_2SO_4 and H_3PO_4 at different pH) has been considered as a simple method to prepare high yield lignin nanoparticles (LNP). Field emission scanning electron microscopy (FESEM), Nano-Zetzsozer (ZS), gel permeation chromatography (GPC) and thermo gravimetric analysis (TGA) have been utilized to determine the influences of the precipitation procedures on particle size, Zeta potential, molecular weight and thermal stability of final obtained LNP. Fourier transform infrared spectroscopy (FTIR), X-ray photoelectron spectroscopy (XPS) and nuclear magnetic resonance (NMR) were also considered to investigate the influences of lignin chemical structures and composition on its antioxidative and antimicrobial behaviours. Results from DPPH (1,1-Diphenyl-2-picryl-hydrazyl) activity revealed the antioxidant response of LNP aqueous solution, whereas results from antimicrobial tests confirmed LNP as effective antibacterial agents against Gram negative bacteria *Pseudomonas syringae* pv. *tomato* (CFBP 1323) (Pst), *Xanthomonas axonopodis* pv. *vesicatoria* (CFBP 3274) (Xav) and *Xanthomonas arboricola* pv. *pruni* (CFBP 3894) (Xap) plant pathogen strains. The results confirmed how high efficient antioxidant and antimicrobial LNP could be considered as an easy methodology for plant pathogens control.

Keywords: nanolignin, high-yield synthesis, acid extraction, plant protection, organic antioxidant

Introduction

Excessive consumption of not renewable fossil resources has caused tremendous rise of harsh problems, like environmental pollution and global warming. Hence, extensive attempts and efforts should be taken to explore and develop new generation of sustainable and energy-saving materials. Lignin, which is the second most abundant natural biomass after cellulose and easily found in the terrestrial plants on earth [1, 2], is a tangible example of these materials. It comprises 20–30 % of woody plant cell walls and, by forming a matrix surrounding cellulose and hemicellulose, it provides strength and protection to the plant. It is a three-dimensional, highly cross-linked macromolecule generally composed by three types of substituted phenols, which include coniferyl (guaiacyl, **G)**, sinapyl (syringyl, **S)**, and p-coumaryl alcohols (hydroxyphenyl, **H)**, yielding a vast number of functional groups and linkages [3-6]. The molecular picture of lignin can be even more complicated due to its chemistry dependence on the source. It can be classified into four categories (i.e. Kraft, lignosulfonate, soda and organosolv lignin, respectively) by sulphur or sulphur-free processes [7]. Kai et al [1] have comprehensively summarized the structures and properties of these four technical lignins.

Quite recently, researchers started to investigate how to use lignin at the nanoscale and many different chemical/physical approaches have been developed to obtain lignin nanoparticles (LNP) from different resources. In 2012, Frangville et al. [8] fabricated novel non-toxic and biodegradable LNP, obtained by precipitation from ethylene glycol via gradual addition of diluted acid aqueous solution, that exhibited size stability upon pH variation. In 2014, Nail et al. [9] produced lignin nanoparticle by high shear homogenization obtaining, after 4h of mechanical shearing, LNP with diameters less than 100 nm, with no major changes in chemical composition, molecular weight and polydispersity between the original kraft lignin particles and the homogenized nanolignin. Qian et al. [10] reported the formation mechanism of uniform colloidal spherical acetylated lignin nanoparticles by self-assembly, obtained by gradual addition of water into acetylated lignin- tetrahydrofuran (THF) solution. In 2015, Gilca et al. [11] also presented a physical ultrasonic irradiation method to produce lignin nanoparticles, which could be explained by two main reaction patterns, i.e. side chain cleavage/depolymerization and oxidative coupling/polymerization. In 2016, Lievonen et al. [12] introduced a straightforward way to isolate spherical lignin nanoparticles by dissolving waste soft wood kraft lignin in THF, followed by introducing water into the system for dialysis process, demonstrating how dispersion stability of the nanoparticles could be influenced by storage time, salt concentration and pH. Myint et al [13] developed a simple one pot green technology to obtain nanoparticles from commercial kraft lignin by using compressed CO_2 antisolvent. Various process parameters (temperature, pressure, solution flow rate and initial solution concentration) were investigated and their effects on product yields, morphology, size, size distribution, surface area and textural properties of the particles were reported, showing how higher temperature and initial lignin concentration induced higher particle aggregation/coalescence degree along with a broader size distribution, which were observed as well when reducing the processing pressure and solution flow rate. Richter et al. [14] synthesized tunable colloidal LNP ranging from 45 to 250 nm based on flash precipitation of dissolved lignin starting from Kraft and Organosolv lignin precursors. Results elucidated that the colloidal stability and dispersion properties are pH and salinities dependent, for example, extending its possible use at extreme pH media. Ago et al. [15] firstly introduced a high-yield preparation technique via a physical aerosol flow reactor for Pickering emulsion utilization, nevertheless, showing unstable size and wide polydispersity (~30 nm to ~2 μm), which limits its utilization. In 2017, Xiong et al. [16] focused on preparing size and shape uniform enzymatic hydrolysis lignin nanospheres (size range of 190–590 nm) by a physical layer-by-layer self-assembly method, identically based on the intrinsic insolubility of lignin in water similar to [10] The chemically stable lignin nanospheres exhibited diameter and yield dependence on initial enzymatic hydrolysis lignin concentration, stirring rate and water dropping rate. Salentinig et al [17] designed the submicron-sized spherical lignin particles by assembly from nanosized lignin upon solvent exchange (from tetrahydrofuran to water) based on the colloidal transformation principle. The lignin particle exhibited strong dependence of surface fractal and stability upon solvent and pH properties, while a gel-like material formed at low pH. Up to now, these novel biodegradable nanolignins have been successfully considered in multiple applications, such as fillers in polymeric nanocomposites [18-25], cosmetics, medical materials [27-29], nano precursor (including nanocapsule, nanocontainer, controlled-release precursor for some functional agents) [14, 30-34], Pickering emulsions [15, 35], carbon (nano)fibers [36, 37], light weight nanomaterials (such as foams and xerogels) for absorption, building and automotive applications [38, 39]. Antioxidative and antimicrobial activity of lignin has been also widely studied for biological applications, and extensively reviewed in [38]. However, the unidentified and complex chemical structures of lignin make difficult to understand and definitely clarify the origin and efficiency of these interesting properties when LNP find application as drug delivery vehicles. Tremendous potential of lignin nanoparticles in drug delivery for agricultural purposes was already demonstrated [31], proving that the abundant biopolymer lignin can be used as an efficient material for the preparation of nanoparticles with variable morphologies and can applied in agriculture as biodegradable drug carrier. LNP were studied with respect to the uptake and the effect on the plant, since lignin is an attractive material for the smart delivery in agriculture as it is enzymatically degradable and it was proved that these nanocarriers can be designed either for hydrophilic or hydrophobic cargos and their nanostructure can be adjusted to tune the release kinetics of pesticides, fungicides [31]. Nevertheless, the possibility of using unmodified precipitated LNP, able to penetrate the epidermis of root tissue, accumulate in root cells, and be transported through the vascular cylinder to leaves still need to be investigated: in particular, the effect of using different acids and different acidic conditions on thermal, morphological, and surface properties of precipitated LNP and their final use as antibacterial agent in plant protection has not been considered yet.

This approach has been already taken into account in the case of cellulose nanocrystals: Espinosa et al. [39] reported about thermal stability of cellulose nanocrystals isolated from HCl, H_2SO_4 and H_3PO_4. Acid concentration and isolation time were considered as variable parameters and results revealed that the cellulose nanocrystals from HCl show the best thermal stability. On the basis of these preliminary results, we followed the same approach in the case of lignin, highlighting how a simple (dissolution of pristine lignin into ethylene glycol [21]), high-yield synthesis procedure can affect size and thermal stability of final obtained LNP when different acidic conditions (HCl, H_2SO_4 and H_3PO_4 at different pH) are considered. Their chemical structures and composition were analyzed in details and their influence on antioxidant and antimicrobial behavior towards bacterial plant pathogens was deeply investigated.

Experimental

Materials: Alkali lignin was supplied by Sigma-Aldrich and used as received. Ethylene glycol, HCl, H_2SO_4 and H_3PO_4 and all the other chemicals used for isolation and purification were purchased from Sigma-Aldrich.

Lignin nanoparticle (LNP) synthesis: LNP suspension was prepared by hydrochloric acidolysis on the basis of methods developed in previous work [21]. In details, a solution of 4 wt. % of lignin in ethylene glycol was prepared and stirred for 1 h at 35 °C, then hydrochloric acid (0.25 M), H_2SO_4

(0.2 M) and H_3PO_4 (0.15 M) were separately added to 96.0 mL of lignin solutions at a rate of 3 drop/min until reaching the set pH values (4.6 and 2.5 for HCl, 4.7 and 2.9 for H_2SO_4, 3.3 and 2.6 for H_3PO_4). The reaction was retained for another 2 h after finishing the addition of the acids. A filtration through a hardened ash less filter paper (Whatman 541, pore size 22 μm) was performed, in order to remove the insoluble impurities from lignin. The solution was then dialyzed against deionized water for three days and a final pH of 7.0 was obtained. The suspension was then diluted into a 400 mL aqueous suspension with deionized water. An ultrasonic treatment by means of a tip sonicator (Vibracell, 750) for 5 min at 40% amplitude was performed in a water-ice bath to prevent overheating. The solid LNP was collected by freeze-vacuum dry method (lyophilizer Virtis B.T. 2K ES).

Nanoparticles Characterization

Scanning Electron Microscopy: Lignin samples were examined by a field emission scanning electron microscope (FESEM, Supra 25-Zeiss) at an operating voltage of 5kV. A drop of lignin water suspensions (pH = 7.0) was cast onto silicon substrate, dried for 24 h and gold sputtered before the analysis. Ninety measurements of nanoparticles diameters were made on FESEM images by means of Nikon NIS-Elements Basic Research (Japan) software.

Zeta potential: Zeta potential measurements were performed on a Nano-ZS Zetzsozer ZEN3600 (Malvern Instruments Ltd., UK) in the deionized water media at pH 7.0 and 0.10 mg/mL of concentration.

Molecular weight (MW) determination: the measurement was performed in accordance with [42] through gel permeation chromatography (GPC) analysis, i.e., the dry pristine and nanosized lignin samples were dissolved in THF solution using an Agilent 1200 series liquid chromatography system equipped with ultraviolet (UV) detector. The dissolved samples were filtered through a 0.45 μm membrane filter before injection and 20 μL were automatically injected. GPC analyses were completed using a UV detector on a 4-column sequence of Waters Styragel columns (HR0.5, HR2, HR4, and HR6) at 1.00 mL/min flow rate. Polystyrene standards were used for calibration. WinGPC Unity software (version 7.2.1, Polymer Standards Services USA, Inc.) was used to collect data and determine molecular weight profiles. The analysis was run in duplicate for every sample.

Fourier transform infrared spectroscopy (FTIR): FTIR spectra of the powdered pristine lignin and isolated lignins were recorded on an FTIR spectrometer, JASCO, 680 plus (Easton, MD 21601

USA). The powders of pristine lignin and LNPs were measured using an attenuated total reflection (ATR) mould method in the range of 4000–400 cm^{-1} wavenumber.

X-ray photoelectron spectroscopy (XPS): The chemical states of the component elements were examined using a AXIS-HSi XPS instrument (Shimadzu/Kratos, Ltd., Japan) equipped with a Mg Kα X-ray source operated at 150 W and a charge neutralizer. Spectra were recorded using an analyzer pass energy of 20 eV and a step size of 0.1 eV per step. The quantification was performed using the default relative sensitivity factor (RSF) values supplied by the XPS manufacturer. Two point energy stable referencing was made using adventitious C (284.5 eV) and valence bond energy corrections. The percentages of individual elements detection were determined from the relative composition analysis of the peak areas of the bands.

Nuclear magnetic resonance (NMR): NMR spectra were recorded on a Bruker AVANCE 600 MHz spectrometer at 300 K using DMSO-d_6 as the solvent. The testing conditions are referred to the study by EA Capanema et al [43]. For the quantitative ^{13}C NMR, the concentration of lignin was 20%; 90° pulse width, 1.4 s acquisition time and 1.7 s relaxation delay were considered. Chromium(III) acetylacetonate (0.01 M) was added to the lignin solution to provide complete relaxation of all nuclei. A quantitative ^{1}H NMR spectrum of lignin samples was recorded at a lignin concentration of ~2% in DMSO-d_6, with a 90° pulse width and a 1.3 s acquisition time.

Thermal stability: TGA was carried out by using a Thermo gravimetric Analyzer (TGA, Seiko Exstar 6300). The samples, approximately 5 mg, were placed in the furnace and heated from 25 to 800 ˚C at a heating rate of 10 ˚C /min under both nitrogen and air atmospheres. The peak values and the residual weight at the end of the tests were derived from derivative thermogravimetric (DTG) data. Maximum thermal degradation temperature (T_{max}) was also collected from DTG peaks maxima. The tests were repeated three times.

UV-Vis analysis: Absorbance spectra of LNP suspended in water (0.05 g/L) were recorded by using an ultraviolet-visible (UV-Vis) spectrophotometer (Lambda 35). Absorbance within a 300 to 900 nm spectral range was measured at 1 nm spectral resolution. The baseline during the experiment was made using only DI water as reference.

Antiradical activity of lignin: The antiradical activity of lignin solutions was tested by using a spectroscopic method, based on the disappearance of the absorption band at 517 nm of the free radical, 2,2-diphenyl-1-picrylhydrazyl (DPPH) (Sigma-Aldrich) upon reduction by an antiradical compound [44]. The test consisted in adding certain amount of the LNP aqueous solution into 2 mL of a DPPH solution in methanol (25 mg/mol L^{-1}) to have 50 mg/L as concentration of LNP solution in methanol, after that the intensity of the 517 nm absorption band was measured overtime by using a ultraviolet-visible (UV-Vis) spectrophotometer (Varian (Cary 4000, USA)). The antioxidant activity was expressed as the ability to scavenge the stable radical DPPH, which was calculated as radical scavenging activity (RSA) using the following equation (**Equation 1**):

$$(RSA,\%) = \left[\frac{A_{control} - A_{sample}}{A_{control}}\right] * 100 \qquad (1)$$

where $A_{Control}$ and A_{Sample} are the absorbances of the control (methanol) at t = 0 min and tested sample at different incubation times, respectively.

Antibacterial activity of lignin

Assay spot diffusion. Bacterial suspensions were developed by $1x10^6$ UFC/ml of *Pseudomonas syringae* pv. *tomato* (CFBP 1323) (Pst), *Xanthomonas axonopodis* pv. *vesicatoria* (CFBP 3274) (Xav) and *Xanthomonas arboricola* pv. *pruni* (CFBP 3894) (Xap), known bacterial plant pathogens. Under sterile conditions, a specific rate (100 μl) of each bacterial suspension was plated on Petri dishes containing NAS (agar 1.8%, peptone 0.8%, sucrose 5%) medium. Lignin nanoparticle water solutions from HCl precipitation, pH 2.5 (concentrated both at 5% and 8% wt.), four rates, 10 μl each, were plated on NAS medium at the tops of a square and an equal amount of sterile distilled water (SDW) was placed as negative control at the centre of each Petri dish; all tests were replicated three times. The inoculated NAS Petri dishes were then placed at 26 ± 1 °C for 48 h and the appearance of an inhibition halo was verified every 24 h. After 48 h, the spot radius and the inhibition halos were measured. All the results obtained from the various tests were subjected to a statistical analysis (ANOVA).

Assay growth in broth. Optical density at a wavelength equal to 590 nm was measured for each selected bacterial strain (Pst, Xav, Xap), by means of a turbidimeter (Biolog Turbidimeter Model 21907). This measurement allowed to make appropriate serial dilutions by SDW obtaining, for each bacterial strain, a known colony concentration of 1×10^8 CFU/mL. The optical density was different for each bacterial strain; in fact, value of 0.22 for Xav, 0.24 for Xap, and 0.30 for Pst, were respectively measured, after performing previous calibration tests. The bacterial suspensions (1 mL) at a concentration of 1×10^8 CFU/mL were 1/10 diluted in SDW, in order to obtain a bacterial concentration of 1×10^7CFU/mL; 1 mL was then placed into a sterile bacteriological tube, with 9 mL of SDW to obtain 10 mL final suspension of bacterial concentration 1×10^6 CFU/mL. Thesis (sterile tubes, five x thesis) were prepared by considering lignin nanoparticle suspensions at 4% wt.. Nutrient broth (32%) alone was serviced as control. The bacterial solutions at 1×10^6 CFU/mL were incubated on a reciprocal orbital incubator at a temperature of 27 ± 1◦C at 150 g min^{-1}. Subsequently, samples were taken at 1 h, 3 h, 12 h and 24 h after incubation. For each sample, 1 mL per thesis was taken and, in sterile conditions, serial dilutions were conducted. Per each 0.1 mL were plated on a Petri dish containing the medium. The plates were then incubated for 48 h at a 27 ± 1°C; subsequently, the count of developed bacterial colonies was carried out.

Assay incorporation of lignin nanoparticles. The same bacterial strains used in spot diffusion tests were considered and bacterial suspensions of $1x10^4$ CFU/mL, $10x10^5$ CFU/mL and $1x10^6$ CFU/mL under sterile conditions were considered. 10 μl of each bacterial suspension was placed on Petri dishes containing a NAS medium and the tests were conducted for pristine lignin (4% wt.), and LNP isolated at lower pH (LNP isolated by H_3PO_4 (pH 2.6) (4% wt.), LNP isolated by H_2SO_4 (4% wt.) (pH 2.9), LNP isolated by HCl (4% wt.) (pH 2.5)) and compared with control (specific bacteria (Pst, Xav, Xap). All tests were replicated three times.

Results and discussion

Physical tests (size, yield, zeta potential and molecular weight): The optimized preparation procedures resulted in high yield of the final LNP content up to 87.9, 85.4 and 78.5% for HCl, H_2SO_4 and H_3PO_4 acidolysis, respectively. The yield (Y, %) was calculated according to $Y=((c_{LNP} *W_s)/W_i)*100$, where c_{LNP} is the concentration of the LNP suspension, W_s is the total weight of the diluted LNP suspension and W_i is the initial weight of microlignin. Obviously, alkali lignin well dissolves into ethylene glycol, due to the strong hydrogen bonds between them, but results not soluble in water media [45]. Consequently, the amount of acids addition (i.e. the pH values) could influence the final yield of lignin nanoparticles. **Figure 1** shows FESEM images of clustered lignin nanoparticles, with evidence of a glued substance, which was believed to be ethylene glycol linked with lignin, observed in the case of lignin HCl 4.6 and H_2SO_4 4.7. Size distribution analysis (**Table 1**) revealed that, after the acidolysis, the diameter of the lignin nanoparticles was pH-value dependent, mainly in the range of 25-50 nm for HCl and 50-80 nm for H_2SO_4 and H_3PO_4 treated lignin, with average values of 32.8±6.0 for HCl 2.5, 58.9±8.6 for H_2SO_4 2.9 and 54.1±6.7 nm for H_3PO_4 2.6, respectively. The measured Zeta potential values for LNPs samples were lower than

-30.0 mV, due to the high number of phenolic moieties, which undergo a proton coupled electron transfer mechanism, namely the high presence of O-containing groups on the lignin surface. It is worthwhile noticing that lignin nanoparticles can be very stable for more than 1 year in an aqueous ambient at 5 °C without observing any precipitated dot, behaviour which is attributed to the electrostatic repulsions between negatively charged LNPs, resulting in electrosteric stabilization. The acid hydrolysis treatment on the pristine lignin caused a decline of the average molar mass (M_n) (**Table 1** and **Figure S1**) of the final lignin nanoparticles, inducing a broader polydispersity index, which suggests an abundance in lower molecular weight particles.

FTIR: **Figure 2a** shows the typical chemical structure of lignin unit and FTIR results in the range of 2000-650 cm^{-1} wavelength scale, before and after hydrochloric acid hydrolysis process (similar results were obtained in the case of sulfuric and phosphorous acids treatments, see **Figure S2**). The abundance in absorption peaks exhibited in the FTIR spectra also demonstrated the structural intricacy and inhomogeneity of lignin. Compared to the pristine lignin, the acid treated lignin maintained the peaks at 700-850, 1032, 1131, 1217, 1266, 1368, 1426, 1460 and 1514 cm^{-1}, suggesting that the acid treatment could preserve most of the functional groups in alkali lignin, and the "core" of the lignin structure did not change significantly. The bands from 1450 to 1600 cm^{-1} multiple peaks are associated with C=C stretching in aromatic ring, and the band from 1030 to 1100 cm^{-1} are assigned to C−O deformation in secondary alcohol and alicyclic ethers [13]. The band at ~1032 cm^{-1} in pristine lignin represents the aromatic C−H in-plane deformations of ***S*** unit, which was shifted towards lower wavelength (1028 cm^{-1}) in the case of LNP (HCl 2.5), which indicates an increasing content of ***S*** units after acidolysis process in comparison with pristine lignin [46, 47]. The slight shift towards lower wavelength of peaks identified at wavenumbers lower than 850 cm^{-1}, associated to aromatic C-H out of plane deformation of ***S*** and ***G*** units, confirmed the observation. The band at ~ 1267 cm^{-1} assigned to C−O stretching in the alkoxy functional group, which is related to the stretching in guaiacyl (***G***), still shows high intensity [48], which contributes on enhancing the solubility and stability of lignin nanoparticles [13]. The vibration at 1217 cm^{-1} is common for the spectra of all lignins and can be associated to C-C, C-O and C=O stretching [49].

The sharp peak at 1540 cm^{-1} should be assigned to the presence of residual ethylene glycol, which disappeared when pH decreases to 2.5. Both conjugated (1693 cm^{-1} due to carboxyl groups C=O stretching in an *α, β*- unsaturated aldehyde or ketone) and unconjugated (1633 cm^{-1}) carboxyl groups in the LNPs sample can be also observed, while conjugated carboxyl groups (1650 cm^{-1}) were prominent compared to pristine lignin [46,50]. The new emerging peak at 1710 cm^{-1} of LNP (HCl 2.5) should be assigned to the conjugated aromatic ketones (Ar-C=O) or esters bonds [51].

^{1}H and ^{13}C NMR: Lignin structure complexity is well-known, which depends on the resource of lignocellulosic biomass. Furthermore, the plenty of pretreatment technologies increases the structure complexity of the biomass lignin [46, 52]. **Figure 2b** lists the typical structure of alkali lignin (**Figure 2b_A**) and some of its derivatives (**Figure** 2b**_B, 2b_C, 2b_D**). **Table 2** and **Figure 2c** summarize the results of ^{1}H NMR integrated peak area regions assigned to functional groups [51, 53, 54]. The composition of aliphatic bonds at 2.25 ppm (–C–CH_2–C, –C–CH_3) and 6.00–4.05 ppm (–CH–O) maintained steady, in the meanwhile the 3.0-4.05 ppm peak, due to the substitution of methoxyl group (−OCH_3) in the aromatic ring [48, 55], evidently increases implying the formation of more ***H*** and ***G*** units transfer to ***G*** and ***S*** units. The declined contents on aromatic (6.00-8.00 ppm) and phenolic groups (8.00-9.35 ppm) imply that the aromatic rings were possibly oxidized to quinones rings (Ar=O) (**Figure 2b_A'**) [29, 51]. Additionally, the small signal at 8.7 and 9.03 ppm is attributed to the carbonyl groups (−C=O) in aldehydes, such as cinnamaldehyde and benzaldehyde structures [55]. The decrease of peaks assigned to the aldehyde (−CHO) group at 9.77 ppm during the acid treatment procedure demonstrated that some ester bonds (O−C=O) or carboxyl groups (HO−C=O) formed, as confirmed in the increase intensity of peak 3.9 ppm (Ar/R−$COOCH_2$R/Ar) (**Figure 2b_B'** and **Figure 2b_C'**) [48]. The quantitative analysis determined by ^{1}H NMR results confirmed the functional groups change, thus contributing to a better understanding of structure and properties variation.

^{13}C NMR tests (**Figure 2d**) were also performed to provide more information of chemical analysis of lignin before and after acid hydrolysis in terms of moieties types and relative C amount (**Table 2**). Peaks in the range of 160-140 ppm are typically corresponded to $C_{Ar\text{-}O}$, while 140−123 ppm was assigned to C_{Ar-C}, 123−102 ppm was related to C_{Ar-H} and the spectra band 58−54 ppm was associated to methoxy group, respectively [42, 54], in agreement with observation made with ^{1}H NMR results. There is the appearance of a peak at 62.80-62.90 ppm after treatment with acids, assigned to aliphatic C-γ.

XPS: Quantitative X-ray photoelectron spectroscopy (XPS) was used to determine the elemental composition of pristine lignin and acid treated lignin nanoparticles in various pH media. Results of

C 1s, O 1s and S 2p core levels spectra and elemental compositions calculated from spectra are presented **Table 3**. With increase of acids amount (lower pH value), the sulphur composition decreases from 0.70% to lower content, and the carbon composition increases gradually, along with the weakening of the oxygen composition. Consequently, the C/O ratio between the pristine lignin and acid isolated lignin increases, probably due to the selective substitution of methylol by ethylene glycol during the dissolving process [56]. The fitting data of core level of C 1s and O 1s spectra peak area regions for the pristine and acid hydrolyzed lignin nanoparticles at different pH are presented in **Figure 3**. The fitted C 1s spectra should be corresponded to C1 (C−H, C−C), C2 (C−O) and C3 (including C=O, O=C−O, Ar=O and Ar−C=O) groups bonds. The fitted O1s spectra should be assigned to O1 (O−C), O2 (including C=O, O=C−O, Ar=O and Ar−C=O bonds) [13, 57]. These bonds containing hydroxyl, methoxyl, carbonyl and carboxyl, ether and ester groups are consistent with the lignin structure [58]. Results of the composition C1, C2, C3 and O1, O2 summarized from fitting spectra peak area regions are even presented in **Table 3**. The spectra clearly illustrate significant changes in chemical functions of lignin surface before and after acid treatment process. The lignin nanoparticles isolated at higher amount of acids (lower pH) resulted with lower C2 and higher C3 content (i.e. lower O1 and higher O2 content), suggesting C2 transfer to C3 bonds with formation of ester and quinone groups, and then confirming consistence with the FTIR, ^{1}H and ^{13}C NMR results.

TGA: In order to investigate the effect of acid amount/type on thermal degradation behaviour of solid lignin, TG and DTG curves were recorded both in inert (**Figure 4a,b)** and oxidative environments (**Figure 4c,d**). The peak values of DTG and the residual weight at 800 °C, were also summarized in **Table 4.** For the lignin extracted at pH values above 3.0 (HCl 4.6, H_2SO_4 4.7 and H_3PO_4 3.3), there are three steps of weight loss during the thermal degradation, the small weight loss (peak 1) at 50-60 °C is due to the loss of adsorbed water. The second weight loss (peak 2) at 140-160 °C was attributed to the thermal degradation of ethylene glycol, which is strongly linked to lignin by internal H-bonding even after dialysis process, (ethylene glycol shows a single degradation peak in this temperature region, as reported in [45]). Residual ethylene glycol was also observed as glued substance in SEM tests (as already observed in (**Figure 1**) and FTIR measurements (**Figure 2a**). The maximum weight loss (peak 3) at 370-380 °C was attributed to the thermal degradation of lignin. For the solid lignin extracted from pH below 3.0 (HCl 2.5, H_2SO_4 2.9 and H_3PO_4 2.6), the second peak disappears, indicating that the H-bonding between lignin and ethylene glycol was interrupted by the acidolysis effect, as a result no ethylene glycol-lignin binding exists, which was also confirmed by the case of H_3PO_4 3.3, with lower intensity of peak 2. These results demonstrated that pure lignin nanoparticles could be obtained at pH values below 3.0. However, the amount of acids seemed not to influence the degradation procedures, as no changes could be observed in peak values except the residual weight. **Table 4** also summarizes the final residue weight of lignin nanoparticles, showing that the LNP extracted by H_3PO_4 2.6 has the highest weight residue (48.7% at 800 °C), with respect of HCl 2.5 (43.0%) and H_2SO_4 2.9 (42.6%) cases. This result is interesting, since the LNP H_3PO_4 2.6 actually exhibits more brightness (whiteness) when compared with the others, possibly responsible for the removal of some chromophore groups in lignin (adjacent quinonoid and para-quinonoid as hints of redness and yellowness) [59]. This phenomenon was also observed under the UV irradiation treatment of lignin THF solution [29]. The other reason was possibly attributed to the high C1 composition derived from XPS, which was easier carbonized than C2 and C3 during thermal decomposition process under nitrogen. Consequently, the thermal stability was enhanced. As detectable in UV Vis spectra (**Figure S3**), lignins obtained at lower pH have higher "brightness", being the colour degree of sample related to the chromophores absorbance at 400–550 nm[60-61]. A variety of chromophores can be introduced into the structure via the nanolignin isolation procedure, one of them is represented by formation of quinone methides and quinones [62]. As alreadyobserved, declined contents on aromatic and phenolic groups in NMR and C2 transfer to C3 bonds in XPS have been detected, confirming the creation of quinones structures. When heated in an inert environment, radicals can be stabilized and trapped by steric factors within the network of lignin and might be triggered at these temperatures. Quinone intermediates could undergo a sort of re-aromatization process, as commented in a recent paper [63], that can explain the higher thermal stability, in inert environment, of low pH treated LNP with respect of higher pH treated LNP.

Figures 4c,d summarize the data of thermal decomposition behaviour of solid lignin under air atmosphere. Evidently, the solid lignins extracted from pH below 3.0 (HCl 2.5, H_2SO_4 2.9 and H_3PO_4 2.6) show higher residue mass than those lignins extracted from pH above 3.0 (HCl 4.6, H_2SO_4 4.7 and H_3PO_4 3.3) due to the residual ethylene glycol, while lignin HCl 2.5 shows highest residue mass 18.6% at 800 °C. The decomposition temperature in air was higher than decomposition temperature in nitrogen environment for the solid lignin powder. The decomposition temperature for solid lignins extracted from acids pH above 3.0 (HCl 4.6, H_2SO_4 4.7 and H_3PO_4

3.3) is higher than those pH below 3.0 (HCl 2.5, H_2SO_4 2.9 and H_3PO_4 2.6). The reason may be attributed to the higher specific surface area for smaller size lignin nanoparticles, which are more accessible to heat resource.

Antiradical activity: Radicals originating from oxygen exist naturally in the atmosphere or can be created by thermal processing or irradiation [64]. The radical scavenging efficiency of an antiradical substance depends on the rate of hydrogen atom abstraction from the phenyl group and also on the stability of the resulting radical. The antiradical activity of LNP solutions was tested by the DPPH, which is readily available, largely used and already employed for lignin based materials [44, 65-67]. **Figure 5a** and **Table 5** show the scavenging activity of free radical DPPH for 50 mg L^{-1} concentrations of LNP in the methanol/DPPH solution after incubation for 10 min. The results show that DPPH scavenging activity of the both pristine lignin and isolated LNP by acids was strong. The absorbance band at 517 nm decreased while DPPH scavenging activity increased, up to 47.5 and more than 60 % for pristine and isolated LNP after only 10 min of incubation. The antioxidant activity of lignin was determined on the fact that lignin maintains high number of phenolic moieties, which undergo a proton coupled electron transfer mechanism. Some studies have revealed that higher antioxidation effect of lignin requires higher quantity of phenolic hydroxyl and phenolic methoxyl groups, a lower quantity of aliphatic oxygen containing groups (such as hydroxyl groups, carbonyl groups and ester groups), lower molecular weight and narrow polydispersity [66, 68]. During the acidolysis procedure, the molecular weight of lignin decreased, together with more aromatic oxygen (like Ar=O and Ar-C=O) structure forming or ***H*** and ***G*** unit transfer to ***G*** and ***S*** unit. Furthermore, alkali lignin consists of hydroxycinnamic acid derivatives: the antioxidant activity of hydroxycinnamic acid was determined by the quantity of hydroxyl groups in the aromatic ring and *ortho* substitutions with the electron donating methoxy groups, proved in zeta potential tests that showed approximately -30 mV for the studied LNP solution. Meanwhile, taking into consideration the high specific surface area and low spherical lignin nanoparticle size, all of these factors contribute to higher proton capability for the phenyl group of lignin.

Antibacterial activity: Three approaches for evaluation of antimicrobial activity of LNP towards plant pathogens have been developed, i.e. spot diffusion assay, incorporation of lignin nanoparticles assay and growth in broth assay. For spot diffusion assay, lignin nanoparticles (HCl precipitated, pH

2.5) were tested at different concentrations with the purpose to verify if their susceptibility varied respect to the increased concentration of active principle. Obtained results showed that an increased susceptibility was observed for Pst and Xav bacterial strains, when the concentration of lignin nanoparticles increases from 5% to 8% wt. *Pseudomonas syringae* pv. *tomato* resulted the most susceptible at both concentrations of 5% and 8%, recording inhibition halos of 0.28 mm and 0.39 mm, respectively. The lignin nanoparticles showed an activity at 5%; when tested at 8% wt., *Xanthomonas arboricola* pv *pruni* resulted more susceptible than *Xanthomonas axonopodis* pv. *vesicatoria*, by measuring inhibition halo's of 0.36 mm and 0.33 mm, respectively **(Figures 5b** and **Table 6**, images are reported for halo measured at 5%).

Bacterial growth in broth was also considered to kinetically quantify the antibacterial activity of LNP. Results show that the growth rate of all bacteria strains declined when compared with control (**Figure 6a-c**). The Pst, however, showed a different trend respect to the other two bacteria (belonging to the *Xanthomonadaceae* family), and the activity was evident at 12h, with a reduction of 2 log units after 24 h. Xav showed a reduction of 2 log units after 12h, nevertheless seemed to re-grow after 24 h.. Among the selected three bacteria, Xap was the most remarkably reduced (3 log units) after 24 h and this is particularly interesting considering its dangerous role and economic losses on peach, plum, apricot, almond and cherry trees in and outside EU area as quarantine plant pathogen. In the case of assay consisting of lignin nanoparticles incorporation, for all bacterial strains *(Pst, Xav* and *Xap*), used at different concentrations ($1x10^4$ CFU/mL, $1x10^5$ CFU/mL and $1x10^6$ CFU/mL) a total inhibition profile was obtained **(Figure 6d)**.

Some researchers have identified a correlation between antibacterial activity and antioxidant properties of lignin extracts. Dizhbite et al. [66] assumed that there was a relationship between the antibacterial activity of kraft lignin with the activity of radical scavengers of the soluble fraction, even Dong et al. [69] assumed that antibacterial activity of lignin extract from corn straw corresponded with its antioxidative activity. As discussed above, antioxidant effects of lignin are related to the scavenging action of their phenolic moieties containing free reactive radicals [70], such as non-etherified hydroxyl phenolic and ortho-methoxy groups. The inhibiting capacity of lignin against several microorganisms growth has been widely reported [67]. This type of alteration was also observed by Rahouti et al.[71], who asserted that when some strains were grown in presence of phenolic substrates some physiological changes occurred (fructification changes, abnormal production of pigments or of viscous compounds). Some authors [73, 74] reported phenolic components of lignin are capable to inhibit some enzymes behaviour and the growth of microorganisms such as *Escherichia coli*, *Saccharomyces cerevisiae*, *Bacillus licheniformis* and *Aspergillus niger*. These authors also commented that side chain structure and nature of the functional groups of the phenolic compounds are major determinants of the antimicrobial effects of lignin: in general, phenolic components with functional groups containing oxygen (such as hydroxyl groups, carbonyl groups and ester groups) in the side chain are less inhibitory, which is consistent with the antioxidant behavior, whereas the presence of double bonds and methyl groups ($–C–CH_3$) increases the biocide effect of phenolics. The present studies pointed out that LNP extraction process can influence chemical structures, purity and molecular weight of obtained product, so side chain structure and nature of the functional groups of the phenolic compounds are major determinants of the antioxidant and antimicrobial lignin behaviour. Actually, the the composition of aliphatic methyl groups kept steady (given in **Table 2**) after acid treatment as measured in ^1H NMR test assigned as 2.25 ppm, suggesting that the acid treatment has no significant impact on the anti-microorganism efficiency of LNP. However, the higher purity, higher surface area and smaller size of LNP would be beneficial to enhance the anti-microorganism behaviour than pristine one.

Figure 7 presents two possible involved mechanisms able to explain antibacterial behavior of extracted LNP, connected to chemistry and lignin shape: firstly, polyphenols cause damage to the cell wall by its lysis, resulting effective in the leakage of the internal fluid [75]. It was supposed that there were numbers of reactive oxygen species (ROS) (absorbed by the polyphenol compounds) aggregated on the surface of LNP due to the high anti-oxidation behavior, which could release and induce oxidative stress by altering the normal redox physiological process when contacting the bacterial. This result remarks that lignin's antioxidant activity coincides with its antibacterial properties by ROS production [76, 77]. In addition, nanoparticles through their small size can penetrate into the bacterial cell, eluding the cell membrane (i.e. Trojan horse mechanism). In this process, some monophenolic compounds originated from lignin such as cinnamaldehyde can deplete adenosine triphosphate (ATP) by infiltrating the bacteria and decreasing the intracellular pH [78]. As a result, the cells die.

Conclusions

Spherical lignin nanoparticles (LNP) were prepared via a simple method by dissolution of pristine alkali lignin into ethylene glycol, followed by addition of different acidic conditions (HCl at pH 4.6 and 2.5, H_2SO_4 at pH 4.7 and 2.9, H_3PO_4 at pH 3.3 and 2.6, respectively). The highest yield at 87.9 wt% of LNP was realized by acid hydrolysis through HCl when the pH value reached 2.5. The results demonstrated that the different acidic conditions dramatically influence the physical properties. In particular, the average diameter of the nanoparticles was found to be pH dependent and well distributed, and the average diameters of the obtained LNP are 32.8±6.0 (HCl pH 2.5), 58.9±8.6 (H_2SO_4 pH 2.9) and 54.1±6.7 nm (H_3PO_4 pH 2.6), respectively. Molecular weight and Zeta potential were also decreased due to the high number of phenolic moieties, which undergo a proton coupled electron transfer mechanism, resulting in the formation of a steady suspension for more than 1 year. Antioxidative and antimicrobial activities of lignin have been studied for potential biological applications. However, the unidentified and complex chemical structures of lignin make difficult to understand and definitely clarify the origin and efficiency of these interesting properties. Higher antioxidant response by DPPH (1,1-Diphenyl-2-picryl-hydrazyl) activity of LNP aqueous solution (50 mg/L) with respect of pristine lignin was revealed, while results from antimicrobial tests confirmed LNP as effective antibacterial organic materials against Gram negative bacteria Pst, Xav and Xap pathogen strains after the systematical evaluation by developing three approaches of antimicrobial activity, i.e. spot diffusion assay, incorporation of lignin nanoparticles assay and growth in broth assay. The results revealed that the chemical structure and composition on lignin surface were significantly impacted during the acid hydrolysis process, nevertheless seems non-related to the used acid. During the acid treatment procedures, aromatic rings of lignin are stable, whereas the methoxyl group ($-OCH_3$) in the aromatic ring and C3 content (including Ar=O and Ar−C=O groups) increased as confirmed by FTIR, ^1H NMR, ^{13}C NMR and XPS, which would enhance the proton coupled electron transfer capacity of lignin phenolic moieties. Furthermore, the *ortho* substitutions with the electron donating methoxy groups together with high specific surface area and low spherical lignin nanoparticle size contribute to higher antioxidative performance of LNP. It was supposed there was a relationship between antibacterial activity and antioxidant property of lignin from the points of view of chemical structure composition. The lignin polyphenols cause damage to the cell wall by the lysis effect, resulting in the leakage of the internal fluid. Meanwhile, some monophenolic compounds originated from lignin such as cinnamaldehyde due to the small size of LNP can penetrate and deplete adenosine triphosphate (ATP) of the cell. Summarizing, it was observed that LNP obtained from HCl 2.5 condition has highest yield (87.9%±0.6), smallest size (32.8 ± 6.0 nm) and improved thermal stability (18.6% residual mass at 800 °C at air condition), while the transfer of H and G units to G and S units detected from FTIR, ^{1}H NMR and ^{13}C NMR suggested the formation of more methoxy groups in LNP structure under condition pH<3.0, responsible of higher antioxidative and antibacterial performance of LNP.

Acknowledgements

Weijun Yang appreciates the funding support from China Scholarship Council (CSC No. 201306600002).

Supporting Information

Figure S1: Representative GPC chromatograms for the pristine, HCl 2.5, H2SO4 2.9, H3PO4 2.6 lignin

Figure S2: FTIR spectra of pristine and acid treated (low pH) lignins

Figure S3: UV-Vis spectra of pristine and acid treated (low pH) lignins

References

1. Kai, D.; Tan, M. J.; Chee, P. L.; Chua, Y. K.; Yap, Y. L.; Loh, X. J., Towards lignin-based functional materials in a sustainable world. *Green Chem.,* **2016**, 18, 1175-1200.
2. Laurichesse, S.; Avérous, L., Chemical modification of lignins: Towards biobased polymers. *Prog. Polym. Sci.,* **2014**, 39 (7), 1266-1290.
3. Saito, T.; Brown, R. H.; Hunt, M. A.; Pickel, D. L.; Pickel, J. M.; Messman, J. M.; Baker, F. S.; Keller, M.; Naskar, A. K., Turning renewable resources into value-added polymer: development of lignin-based thermoplastic. *Green Chem.,* **2012**, 14 (12), 3295-3303.
4. Fortunati, E.; Yang, W.; Luzi, F.; Kenny, J.; Torre, L.; Puglia, D., Lignocellulosic nanostructures as reinforcement in extruded and solvent casted polymeric nanocomposites: an overview. *Eur. Polym. J.,* **2016**, 80, 295-316.
5. Sen, S.; Patil, S.; Argyropoulos, D. S., Thermal properties of lignin in copolymers, blends, and composites: a review. *Green Chem.,* **2015**, 17 (11), 4862-4887.
6. Sarkanen, K. V.; Ludwig, C. H., Lignins. Occurrence, formation, structure, and reactions. New York.; Wiley-Interscience: **1971**.
7. Doherty, W. O.; Mousavioun, P.; Fellows, C. M., Value-adding to cellulosic ethanol: Lignin polymers. *Ind. Crop. Prod.*, **2011**, 33 (2), 259-276.
8. Frangville, C.; Rutkevičius, M.; Richter, A. P.; Velev, O. D.; Stoyanov, S. D.; Paunov, V. N., Fabrication of environmentally biodegradable lignin nanoparticles. *ChemPhysChem* **2012**, 13 (18), 4235-4243.
9. Nair, S. S.; Sharma, S.; Pu, Y.; Sun, Q.; Pan, S.; Zhu, J.; Deng, Y.; Ragauskas, A. J., High Shear Homogenization of Lignin to Nanolignin and Thermal Stability of Nanolignin□Polyvinyl Alcohol Blends. *ChemSusChem* **2014**, 7 (12), 3513-3520.
10. Qian, Y.; Deng, Y.; Qiu, X.; Li, H.; Yang, D., Formation of uniform colloidal spheres from lignin, a renewable resource recovered from pulping spent liquor. *Green Chem.,* **2014**, 16 (4), 2156-2163.
11. Gilca, I. A.; Popa, V. I.; Crestini, C., Obtaining lignin nanoparticles by sonication. *Ultrason. Sonochem.,* **2015**, 23, 369-375.
12. Lievonen, M.; Valle-Delgado, J. J.; Mattinen, M.-L.; Hult, E.-L.; Lintinen, K.; Kostiainen, M. A.; Paananen, A.; Szilvay, G. R.; Setälä, H.; Österberg, M., A simple process for lignin nanoparticle preparation. *Green Chem.,* **2016**, 18 (5), 1416-1422.
13. Myint, A. A.; Lee, H. W.; Seo, B.; Son, W.-S.; Yoon, J.; Yoon, T. J.; Park, H. J.; Yu, J.; Yoon, J.; Lee, Y.-W., One pot synthesis of environmentally friendly lignin nanoparticles with compressed liquid carbon dioxide as an antisolvent. *Green Chem.,* **2016**, 18 (7), 2129-2146.
14. Richter, A. P.; Bharti, B.; Armstrong, H. B.; Brown, J. S.; Plemmons, D.; Paunov, V. N.; Stoyanov, S. D.; Velev, O. D., Synthesis and characterization of biodegradable lignin nanoparticles with tunable surface properties. *Langmuir*, **2016**, 32 (25), 6468-6477.
15. Ago, M.; Huan, S.; Borghei, M.; Raula, J.; Kauppinen, E. I.; Rojas, O. J., High-Throughput Synthesis of Lignin Particles (~ 30 nm to~ 2 µm) via Aerosol Flow Reactor: Size Fractionation and Utilization in Pickering Emulsions. *ACS App. Mater. Inter.,* **2016**, 8 (35), 23302-23310.
16. Xiong, F.; Han, Y.; Wang, S.; Li, G.; Qin, T.; Chen, Y.; Chu, F., Preparation and formation mechanism of size-controlled lignin nanospheres by self-assembly. *Ind. Crop. Prod.,* **2017**, 100, 146-152.
17. Salentinig, S.; Schubert, M., Softwood Lignin Self-Assembly for Nanomaterial Design. *Biomacromolecules* **2017**, 18(8), 2649-2653.

18. Yang, W.; Dominici, F.; Fortunati, E.; Kenny, J. M.; Puglia, D., Effect of lignin nanoparticles and masterbatch procedures on the final properties of glycidyl methacrylate-g-poly (lactic acid) films before and after accelerated UV weathering. *Ind. Crop. Prod.,* **2015**, 77, 833-844.
19. Yang, W.; Fortunati, E.; Dominici, F.; Giovanale, G.; Mazzaglia, A.; Balestra, G. M.; Kenny, J. M.; Puglia, D., Effect of cellulose and lignin on disintegration, antimicrobial and antioxidant properties of PLA active films. *Int. J. Biol. Macromol.,* **2016**, 89, 360-368.
20. Yang, W.; Fortunati, E.; Dominici, F.; Kenny, J. M.; Puglia, D., Effect of processing conditions and lignin content on thermal, mechanical and degradative behavior of lignin nanoparticles/polylactic (acid) bionanocomposites prepared by melt extrusion and solvent casting. *Eur. Polym. J.,* **2015**, 71, 126-139.
21. Yang, W.; Kenny, J. M.; Puglia, D., Structure and properties of biodegradable wheat gluten bionanocomposites containing lignin nanoparticles. *Ind. Crop. Prod.,* **2015**, 74, 348-356.
22. Yang, W.; Owczarek, J.; Fortunati, E.; Kozanecki, M.; Mazzaglia, A.; Balestra, G.; Kenny, J.; Torre, L.; Puglia, D., Antioxidant and antibacterial lignin nanoparticles in polyvinyl alcohol/chitosan films for active packaging. *Ind. Crop. Prod.,* **2016**, 94, 800-811.
23. Yang, W.; Fortunati, E.; Dominici, F.; Giovanale, G.; Mazzaglia, A.; Balestra, G.; Kenny, J.; Puglia, D., Synergic effect of cellulose and lignin nanostructures in PLA based systems for food antibacterial packaging. *Eur. Polym. J.,* **2016**, 79, 1-12.
24. Jiang, C. (2013) Nano-lignin filled natural rubber composites: Preparation and characterization, eXPRESS Polymer Letters 7(5):480-493, DOI10.3144/expresspolymlett.2013.44
25. Garcia Gonzalez, M. N., Levi, M., Turri, S. and Griffini, G. (2017), Lignin nanoparticles by ultrasonication and their incorporation in waterborne polymer nanocomposites. J. Appl. Polym. Sci., 134, 45318. doi: 10.1002/app.45318
26. Figueiredo, P.; Lintinen, K.; Kiriazis, A.; Hynninen, V.; Liu, Z.; Ramos, T. B.; Rahikkala, A.; Correia, A.; Kohout, T.; Sarmento, B., In vitro evaluation of biodegradable lignin-based nanoparticles for drug delivery and enhanced antiproliferation effect in cancer cells. *Biomaterials,* **2017**, 121, 97-108.
27. Qian, Y.; Qiu, X.; Zhu, S., Lignin: a nature-inspired sun blocker for broad-spectrum sunscreens. *Green Chem.,* **2015**, 17 (1), 320-324.
28. Qian, Y.; Qiu, X.; Zhu, S., Sunscreen performance of lignin from different technical resources and their general synergistic effect with synthetic sunscreens. *ACS Sustain. Chem. Eng.,* **2016**, 4 (7), 4029-4035.
29. Wang, J.; Deng, Y.; Qian, Y.; Qiu, X.; Ren, Y.; Yang, D., Reduction of lignin color via one-step UV irradiation. *Green Chem.,* **2016**, 18 (3), 695-699.
30. Chen, N.; Dempere, L. A.; Tong, Z., Synthesis of pH-Responsive Lignin-Based Nanocapsules for Controlled Release of Hydrophobic Molecules. *ACS Sustain. Chem. Eng.,* **2016**, 4 (10), 5204-521.
31. Yiamsawas, D.; Baier, G.; Thines, E.; Landfester, K.; Wurm, F. R., Biodegradable lignin nanocontainers. *RSC Adv.,* **2014**, 4 (23), 11661-11663.
32. Li, H.; Deng, Y.; Liu, B.; Ren, Y.; Liang, J.; Qian, Y.; Qiu, X.; Li, C.; Zheng, D., Preparation of nanocapsules via the self-assembly of kraft Lignin: A totally green process with renewable resources. *ACS Sustain. Chem. Eng.,* **2016**, 4 (4), 1946-1953.
33. Richter, A. P.; Brown, J. S.; Bharti, B.; Wang, A.; Gangwal, S.; Houck, K.; Hubal, E. A. C.; Paunov, V. N.; Stoyanov, S. D.; Velev, O. D., An environmentally benign antimicrobial nanoparticle based on a silver-infused lignin core. *Nat. Nanotechnol.,* **2015**, 10 (9), 817-823.
34. Tortora, M.; Cavalieri, F.; Mosesso, P.; Ciaffardini, F.; Melone, F.; Crestini, C., Ultrasound driven assembly of lignin into microcapsules for storage and delivery of hydrophobic molecules. *Biomacromolecules*, **2014**, 15 (5), 1634-1643.

35. Qian, Y.; Zhang, Q.; Qiu, X.; Zhu, S., CO 2-responsive diethylaminoethyl-modified lignin nanoparticles and their application as surfactants for CO2/N2-switchable Pickering emulsions. *Green Chem.,* **2014**, 16 (12), 4963-4968.
36. Lai, C.; Kolla, P.; Zhao, Y.; Fong, H.; Smirnova, A. L., Lignin-derived electrospun carbon nanofiber mats with supercritically deposited Ag nanoparticles for oxygen reduction reaction in alkaline fuel cells. *Electrochim. Acta* **2014**, 130, 431-438.
37. Svinterikos, E.; Zuburtikudis, I., Carbon nanofibers from renewable bioresources (lignin) and a recycled commodity polymer [poly (ethylene terephthalate)]. *J. Appl. Polym. Sci.,* **2016**, 43936 doi: 10.1002/app.43936
38. Del Saz-Orozco, B.; Oliet, M.; Alonso, M. V.; Rojo, E.; Rodríguez, F., Formulation optimization of unreinforced and lignin nanoparticle-reinforced phenolic foams using an analysis of variance approach. *Compos. Sci. Technol.,* **2012,** 72 (6), 667-674.
39. Yang, Y.; Deng, Y.; Tong, Z.; Wang, C., Renewable lignin-based xerogels with self-cleaning properties and superhydrophobicity. *ACS Sustain. Chem. Eng.,* **2014**, 2 (7), 1729-1733.
40. Roopan, S. M., An overview of natural renewable bio-polymer lignin towards nano and biotechnological applications. *Int. J. Biol. Macromol.* **2017**, 103, 508-514.
41. Camarero Espinosa, S.; Kuhnt, T.; Foster, E. J.; Weder, C., Isolation of thermally stable cellulose nanocrystals by phosphoric acid hydrolysis. *Biomacromolecules* **2013**, 14 (4), 1223-1230.
42. Dodd, A. P.; Kadla, J. F.; Straus, S. K., Characterization of fractions obtained from two industrial softwood kraft lignins. *ACS Sustain. Chem. Eng.,* **2014**, 3 (1), 103-110.
43. Capanema, E. A.; Balakshin, M. Y.; Kadla, J. F., A comprehensive approach for quantitative lignin characterization by NMR spectroscopy. *J. Agr. Food. Chem.,* **2004**, 52 (7), 1850-1860.
44. Lu, Q.; Zhu, M.; Zu, Y.; Liu, W.; Yang, L.; Zhang, Y.; Zhao, X.; Zhang, X.; Zhang, X.; Li, W., Comparative antioxidant activity of nanoscale lignin prepared by a supercritical antisolvent (SAS) process with non-nanoscale lignin. *Food Chem.,* **2012**, 135 (1), 63-67.
45. Mu, L.; Shi, Y.; Wang, H.; Zhu, J., Lignin in ethylene glycol and poly (ethylene glycol): Fortified lubricants with internal hydrogen bonding. *ACS Sustain. Chem. Eng.,* **2016**, 4 (3), 1840-1849.
46. Tian, D.; Hu, J.; Chandra, R. P.; Saddler, J. N.; Lu, C., Valorizing recalcitrant cellulolytic enzyme lignin via lignin nanoparticles fabrication in an integrated biorefinery. *ACS Sustain. Chem. Eng.,* **2017**, 5 (3), 2702-2710
47. Gabov, K.; Gosselink, R. J.; Smeds, A. I.; Fardim, P., Characterization of lignin extracted from birch wood by a modified hydrotropic process. *J. Agr. Food. Chem.,* **2014**, 62 (44), 10759-10767.
48. Deepa, A. K.; Dhepe, P. L., Lignin depolymerization into aromatic monomers over solid acid catalysts. *ACS Catal.,* **2014**, 5 (1), 365-379.
49. Lupoi, J.S, Singh, S., Parthasarathi, R., Simmon, B.A., Henry, R.J. Recent innovations in analytical methods for the qualitative and quantitative assessment of lignin, *Renew Sust Energ Rev*, **2015**, 49, 871-906.
50. Li, H.; McDonald, A. G., Fractionation and characterization of industrial lignins. *Ind. Crop. Prod.,* **2014**, 62, 67-76.
51. Cheng, Y.; Zhao, P.-X.; Alma, M. H.; Sun, D.-F.; Li, R.; Jiang, J.-X., Improvement of direct liquefaction of technical alkaline lignin pretreated by alkaline hydrogen peroxide. *J. Anal. Appl. Pyrol.,* **2016**, 122, 277-281.
52. Chandra, R. P.; Bura, R.; Mabee, W.; Berlin, d. A.; Pan, X.; Saddler, J., Substrate pretreatment: The key to effective enzymatic hydrolysis of lignocellulosics? In Biofuels, Springer: 2007; 67-93.
53. Nagy, M.; David, K.; Britovsek, G. J.; Ragauskas, A. J., Catalytic hydrogenolysis of ethanol organosolv lignin. *Holzforschung* **2009**, 63 (5), 513-520.

54. Nagy, M.; Kosa, M.; Theliander, H.; Ragauskas, A. J., Characterization of CO 2 precipitated Kraft lignin to promote its utilization. *Green Chem.,* **2010**, 12 (1), 31-34.
55. Sun, Y.-C.; Wen, J.-L.; Xu, F.; Sun, R.-C., Fractional and structural characterization of organosolv and alkaline lignins from Tamarix austromogoliac. *Sci. Res. Essays* **2010**, 5 (24), 3850-3864.
56. Gupta, A. K.; Mohanty, S.; Nayak, S., Synthesis, Characterization and Application of Lignin Nanoparticles (LNPs). *Materials Focus* **2014**, 3 (6), 444-454.
57. Harb, S. V.; Cerrutti, B. M.; Pulcinelli, S. H.; Santilli, C. V.; Hammer, P., Siloxane–PMMA hybrid anti-corrosion coatings reinforced by lignin. *Surf. Coat. Tech.,* **2015**, 275, 9-16.
58. Gosselink, R.; Snijder, M.; Kranenbarg, A.; Keijsers, E.; De Jong, E.; Stigsson, L., Characterisation and application of NovaFiber lignin. *Ind. Crop. Prod.,* **2004**, 20 (2), 191-203.
59. Lin, S.; Kringstad, K., Photosensitive groups in lignin and lignin model compounds. *Tappi* **1970**, 53, 658-63.
60. Zhang, H.; Bai, Y.; Zhou, W.; Chen, F. Color reduction of sulfonated eucalyptus kraft lignin, *Int. J. Biol. Macromol.,* 97, **2017,** 201-208.
61. Yu, L.; Yu, J.; Mo, W.; Qin, Y.; Yang, D.; Qiu, X. Etherification to improve the performance of lignosulfonate as dye dispersant, *RSC Adv.,* **2016**, 6, 70863-70869.
62. Wang, J.; Deng, Y.; Qian, Y.; Qiu, X., Ren, Y.; Yang, D. Reduction of lignin color via one-step UV irradiation, *Green Chem.,* **2016**, 18, 695, DOI: 10.1039/c5gc02180d
63. Patil, S. V.; Argyropoulos, D. S. Stable Organic Radicals in Lignin: A Review, *ChemSusChem*, **2017**, 10, 3284.
64. López□de□Dicastillo, C.; Pezo, D.; Nerín, C.; López□Carballo, G.; Catalá, R.; Gavara, R.; Hernández□Muñoz, P., Reducing oxidation of foods through antioxidant active packaging based on ethyl vinyl alcohol and natural flavonoids. *Packag. Technol. Sci.,* **2012**, 25 (8), 457-466.
65. Domenek, S.; Louaifi, A.; Guinault, A.; Baumberger, S., Potential of lignins as antioxidant additive in active biodegradable packaging materials. *J. Polym. Environ.,* **2013**, 21 (3), 692-70.
66. Dizhbite, T.; Telysheva, G.; Jurkjane, V.; Viesturs, U., Characterization of the radical scavenging activity of lignins—natural antioxidants. *Bioresource Technol., 2*__004__, 95 (3), 309-317
67. Lens, J.-P.; De Graaf, L.; Stevels, W.; Dietz, C.; Verhelst, K.; Vereijken, J.; Kolster, P., Influence of processing and storage conditions on the mechanical and barrier properties of films cast from aqueous wheat gluten dispersions. *Ind. Crop. Prod.,* **2003**, 17 (2), 119-130.
68. Ugartondo, V.; Mitjans, M.; Vinardell, M. P., Comparative antioxidant and cytotoxic effects of lignins from different sources. *Bioresource Technol.,* **2008**, 99 (14), 6683-6687.
69. Dong, X.; Dong, M.; Lu, Y.; Turley, A.; Jin, T.; Wu, C., Antimicrobial and antioxidant activities of lignin from residue of corn stover to ethanol production. *Ind. Crop. Prod.,* **2011**, 34 (3), 1629-1634.
70. Cotelle, N.; Bernier, J.-L.; Catteau, J.-P.; Pommery, J.; Wallet, J.-C.; Gaydou, E. M., Antioxidant properties of hydroxy-flavones. *Free Radical Bio. Med.,* **1996**, 20 (1), 35-43.
71. Vermaas, J. V.; Petridis, L.; Qi, X.; Schulz, R.; Lindner, B.; Smith, J. C., Mechanism of lignin inhibition of enzymatic biomass deconstruction. *Biotechnol. Biofuels,* **2015**, 8 (1), 217.
72. Rahouti, M.; Steiman, R.; Seigle-Murandi, F.; Christov, L. P., Growth of 1044 strains and species of fungi on 7 phenolic lignin model compounds. *Chemosphere* **1999**, 38 (11), 2549-2559.
73. Qin, L.; Li, W.-C.; Liu, L.; Zhu, J.-Q.; Li, X.; Li, B.-Z.; Yuan, Y.-J., Inhibition of lignin-derived phenolic compounds to cellulase. *Biotechnol. Biofuels,* **2016**, 9 (1), 70
74. Baurhoo, B.; Ruiz-Feria, C.; Zhao, X., Purified lignin: Nutritional and health impacts on farm animals—A review. *Anim. Feed Sci. Tech.,* **2008**, 144 (3), 175-184.
75. Thomas, S.; Shanks, R.; Joy, J., Micro-and Nanostructured Polymer Systems: From Synthesis to Applications. CRC Press: 2016.

76. Stadtman, E. R.; Berlett, B. S., Reactive oxygen-mediated protein oxidation in aging and disease. *Chemical research in toxicology* **1997**, 10 (5), 485-494.

77. Butterfield, D. A.; Kanski, J., Brain protein oxidation in age-related neurodegenerative disorders that are associated with aggregated proteins. *Mech. Ageing Dev.,* **2001**, 122 (9), 945-962.

78. Dumitriu, S., Polymeric biomaterials. CRC Press: 2013; Vol. 1.

Table 1: Particle size. molecular weight distribution and zeta potential values for acid treated lignin solutions at different pH

Lignin	Yield (%)	Particle size (nm)	Mw (Daltons)	Mn (Daltons)	Polydispersity	Zeta potential (mV)
Pristine		Aggregates	59900	52420	1.14	-21.3±3.5
HCl (4.6)	-	120.0 ± 22.3				
HCl (2.5)	87.9±0.6	32.8 ± 6.0	59680	42070	1.42	-32.9±0.3
H_2SO_4 (4.7)	--	73.7 ± 8.2				
H_2SO_4 (2.9)	85.4±1.0	58.9 ± 8.6	60500	41630	1.45	-31.7±0.7
H_3PO_4 (3.3)	--	63.5 ± 8.1				
H_3PO_4 (2.6)	78.5±0.4	54.1 ± 6.7	67310	49680	1.35	-29.8±1.5

Table 2: Hydrogen and Carbon content (%) of pristine and acid treated lignins determined by ^{1}H NMR and ^{13}C NMR

Samples	**Chemical shift (ppm)**					
	2.25~ 0.00	4.05~ 3.0	6.00 ~ 4.05	8.00 ~ 6.00	9.35 ~ 8.00	10.10 ~ 9.35
Assignment	Aliphatic C–CH_2–C. C–CH_3	Methoxyl –OCH_3	Aliphatic CH-O	Aromatic.vinyl CH=CH. CH_2=CH	Phenolic =HC–OH	Formyl –C(O)H
Pristine	12.67	40.64	13.07	25.65	6.91	1.06
HCl (2.5)	12.52	46.77	13.09	22.60	4.48	0.55
H_2SO_4 (2.9)	12.17	46.25	12.97	22.37	5.15	1.10
H_3PO_4 (2.6)	12.81	48.61	11.93	22.24	4.17	0.24
			Chemical shift (ppm)			
	160-140	140-123	123-102	63.8-59.0	58.0-53.0	160-140
t	Phenolic C_{Ar}-O	Aromatic,vinyl C_{Ar}-C, C_{Ar}-H	Aliphatic C-γ	Methoxyl –OCH_3		Phenolic C_{Ar}-O
Pristine	13.82	19.14	38.56	4.37	24.11	13.82
HCl (2.5)	7.51	15.78	38.40	5.69	32.62	7.51
H_2SO_4 (2.9)	7.13	18.25	37.70	6.71	30.21	7.13
H_3PO_4 (2.6)	7.75	16.83	40.91	5.47	29.04	7.75

Table 3: Results of C 1s. O 1s and S 2p core levels spectra and elemental compositions calculated from spectra for pristine and acid treated lignins (Composition of C. O. S and C/O ratio. C1. C2. C3 and O1 and O2 determined from the fitting data)

	C (%)	**O (%)**	**S (%)**	**C/O ratio**	**C1 (%)**	**C2 (%)**	**C3 (%)**	**O1 (%)**	**O2 (%)**
Pristine	74.87	24.44	0.70	3.06	52.9	39.9	7.2	90.1	9.9
HCl (4.6)	75.9	23.5	0.37	3.23	56.1	38.4	5.5	84.8	15.2
HCl (2.5)	77.16	22.26	0.36	3.47	66.6	24.5	8.9	52.0	48.0
H_2SO_4 (4.7)	76.87	22.51	0.38	3.41	56.1	38.4	5.5	84.8	15.2
H_2SO_4 (2.9)	78.46	21.3	0.24	3.68	59.6	29.7	10.7	59.1	40.9
H_3PO_4 (3.3)	76.58	23.26	0.16	3.29	61.8	26.9	11.3	52.9	47.1
H_3PO_4 (2.6)	77.07	22.75	0.18	3.39	66.6	22.2	11.3	49.4	50.6

Table 4: Peak values of DTG and residual weight at 800 °C in nitrogen and air atmospheres for the lignin extracted at different pH values

	nitrogen				air	
Lignin	**Tp_1 (°C)**	**Tp_2 (°C)**	**T_{max} (°C)**	**Residue@ 800 °C**	**T_{max} (°C)**	**Residue @ 800°C**
Pristine	68.3±0.8	157.7±1.0	370.4±0.8	39.7±1.3	458.8±2.1	0.23±0.02
HCl (4.6)		142.8	378.9	37.6	388.7±0.5	3.3±0.2
HCl (2.5)	56.6±0.7		373.3±1.3	43.0±2.2	380.7±3.5	18.6±1.3
H_2SO_4 (4.7)	55.0	141.3	375.9	37.8	445.6±1.6	4.7±0.8
H_2SO_4 (2.9)	57.5±2.0		375.4±2.0	42.6±3.4	385.2±4.0	7.1±0.5
H_3PO_4 (3.3)	50.5	158.2	355.5	36.8	350.2±2.9	3.8±0.0
H_3PO_4 (2.6)	58.1±0.2		377.5±2.5	48.7±1.6	387.2±2.4	12.4±0.2

Table 5: Scavenging activity of free radical DPPH for 50 mg L^{-1} concentrations of LNP in the methanol/DPPH solution after incubation for 10 min.

Lignin	Absorption @ λ=517nm (%)	RSA (%)
Control	39.14	0
Pristine	20.56	47.5
HCl (2.5)	13.91	64.5
H_2SO_4 (2.9)	15.75	59.6
H_3PO_4 (2.6)	13.12	66.5

Table 6: Inhibition halo's with LNP (HCl (2.5), 5% and 8% wt) by spot diffusion test. Bacterial concentration 1 x 10^6 CFU/ml.

Bacteria	**Lignin nanoparticle, 5%wt. (mm)**	**Lignin nanoparticle, 8% wt. (mm)**
Pseudomonas syringae pv. tomato	0.28 ±0.02	0.39 ± 0.02
Xanthomonas axonopodis pv. vesicatoria	0.26 ± 0.01	0.33 ± 0.01
Xanthomonas arboricola pv. pruni	0.24 ± 0.01	0.36 ± 0.02

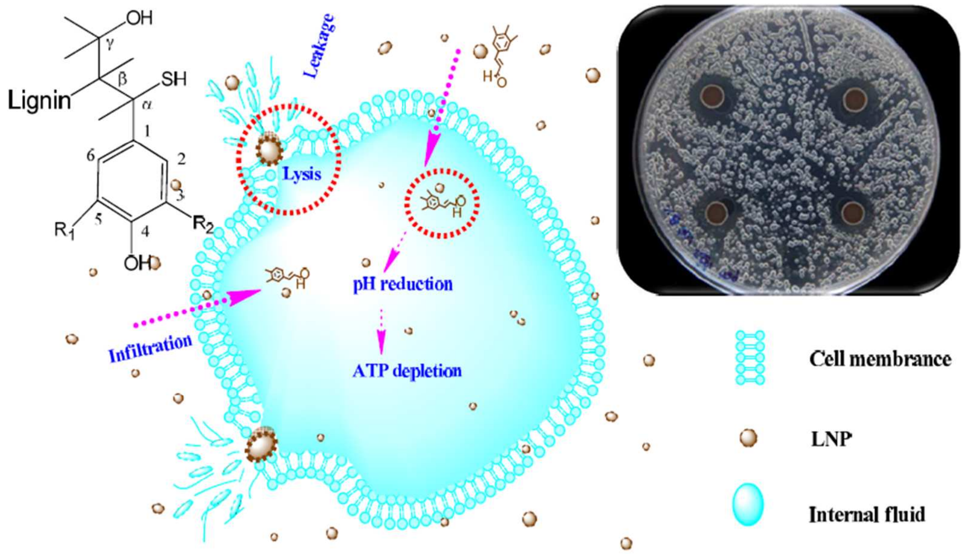

For Table of Contents Use Only

LNPs penetrate the cell wall by its lysis, react with ROS species inducing oxidative stress, ATP depletion and decrease of intracellular pH of plant bacteria.

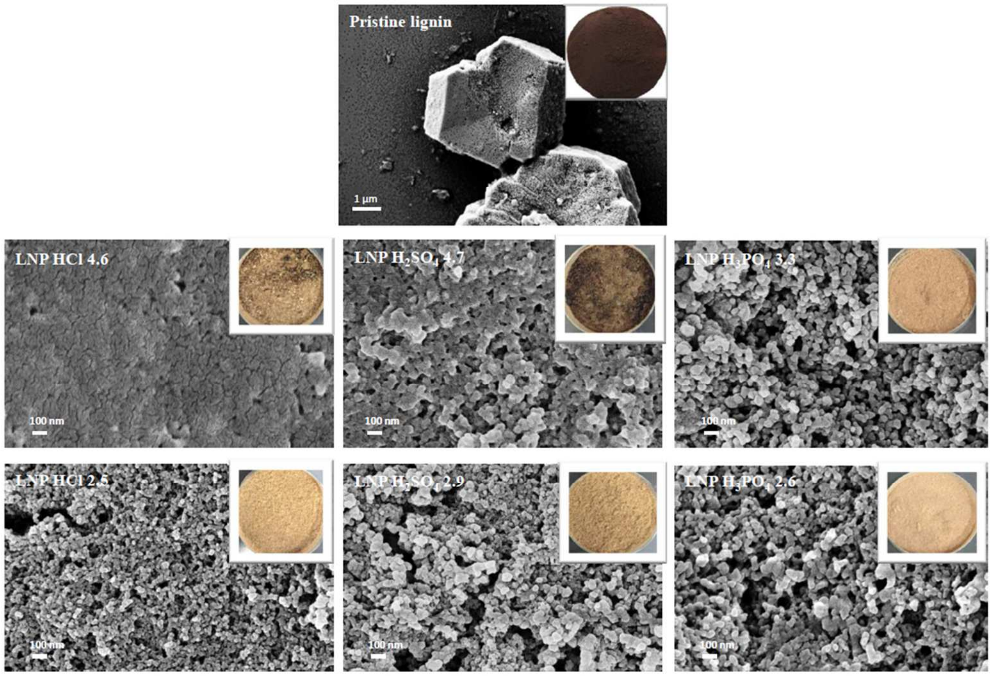

Figure 1: FESEM images of clustered structured lignin nanoparticles after acidolysis.

285x196mm (96 x 96 DPI)

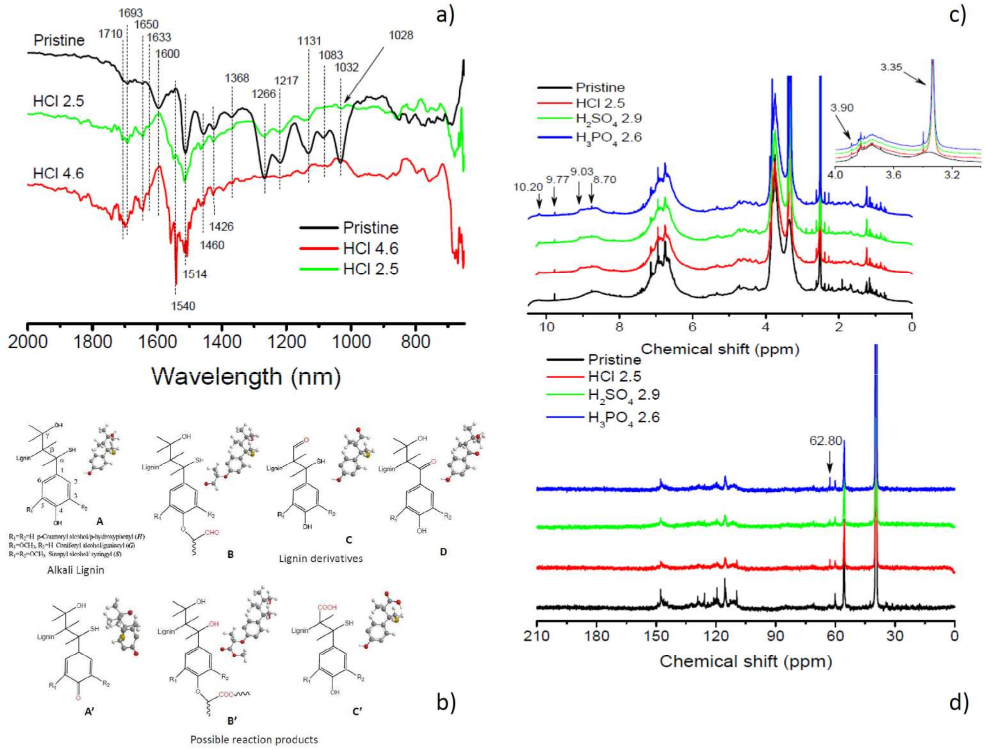

Figure 2: FTIR results in the range of 2000-650 cm-1 wavelength scale, before and after hydrochloric acid hydrolysis process (a); typical structure of alkali lignin (Figure A) and some of its derivatives (Figure B, C, D) (b); 1H and 13C NMR spectra of alkali lignin and LNP after acid treatment (c) and (d).

571x435mm (96 x 96 DPI)

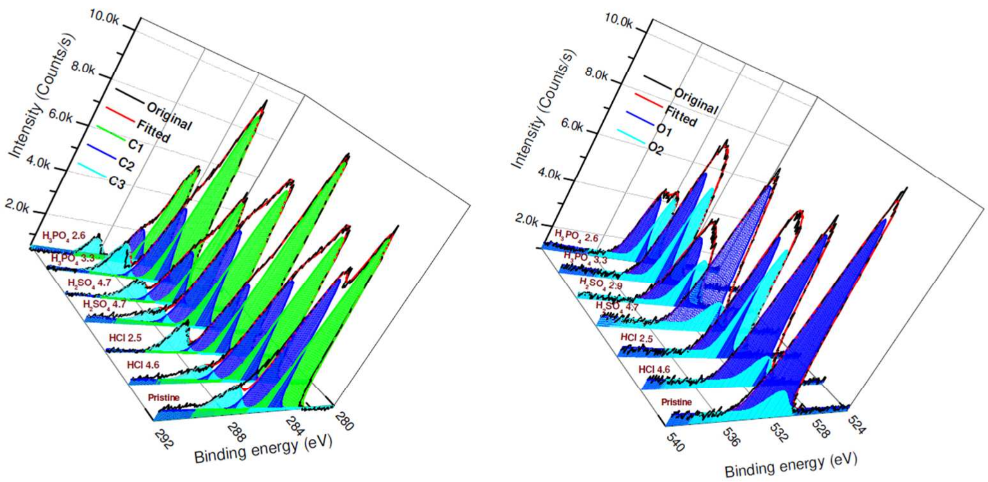

Figure 3: Fitting data of core level of C 1s and O 1s spectra peak area regions for the pristine and acid hydrolyzed lignin nanoparticles at different pH

353x186mm (96 x 96 DPI)

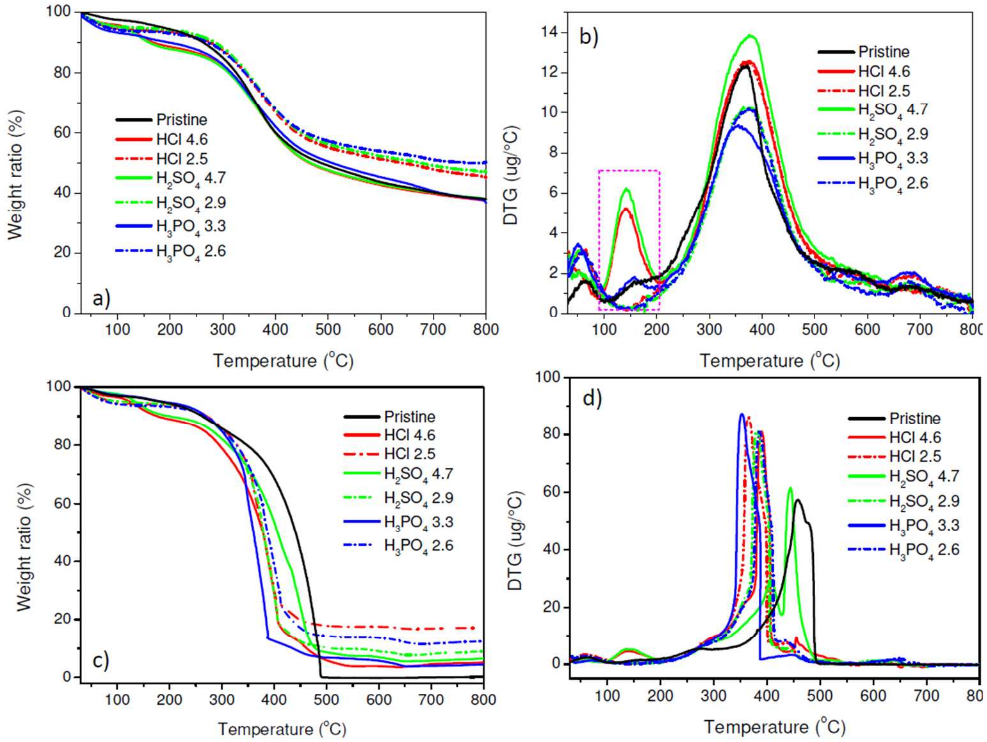

Figure 4: TG and DTG curves of LNP extracted at different pH in (a,b) nitrogen and (c,d) air atmosphere.

298x222mm (96 x 96 DPI)

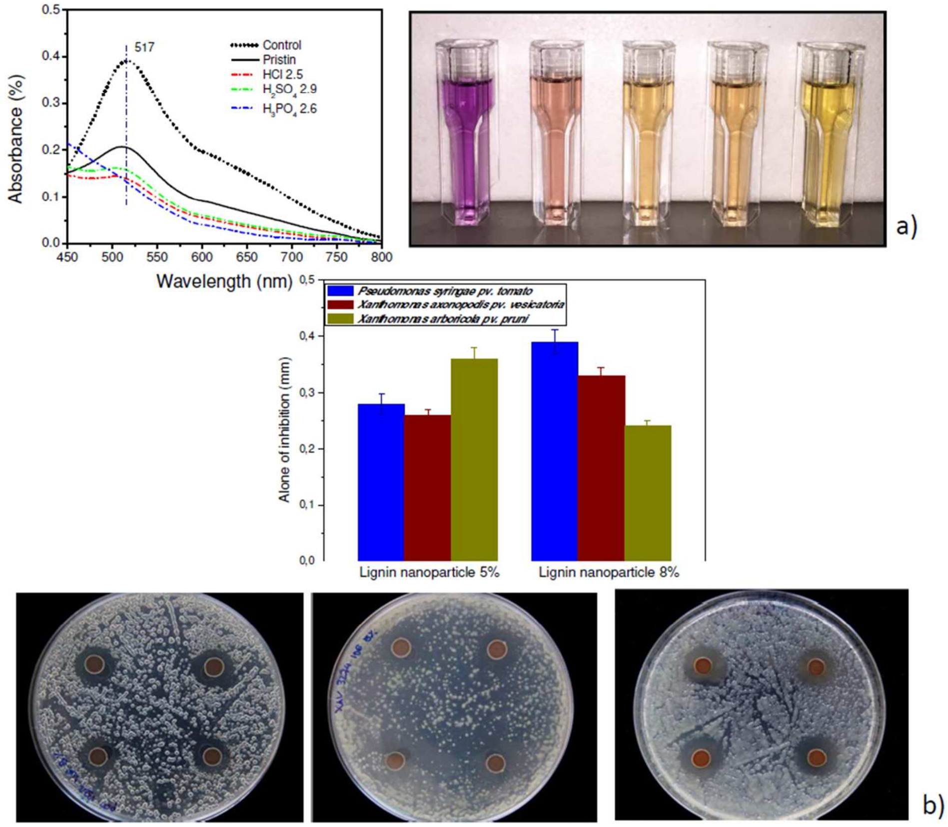

Figure 5: Antioxidant activities of migrating substances for LNP in the methanol/DPPH solution after incubation for 10 min: monitoring of the absorbance for band at 517 nm and colour variation of the DPPH methanol solution (a) and spot diffusion assay of lignin nanoparticles (HCl precipitated, pH 2.5) tested at 5% and 8% towards Pseudomonas syringae pv. Tomato, Xanthomonas arboricola pv pruni and Xanthomonas axonopodis pv. vesicatoria inhibition halo measured at 5% (b).

253x214mm (96 x 96 DPI)

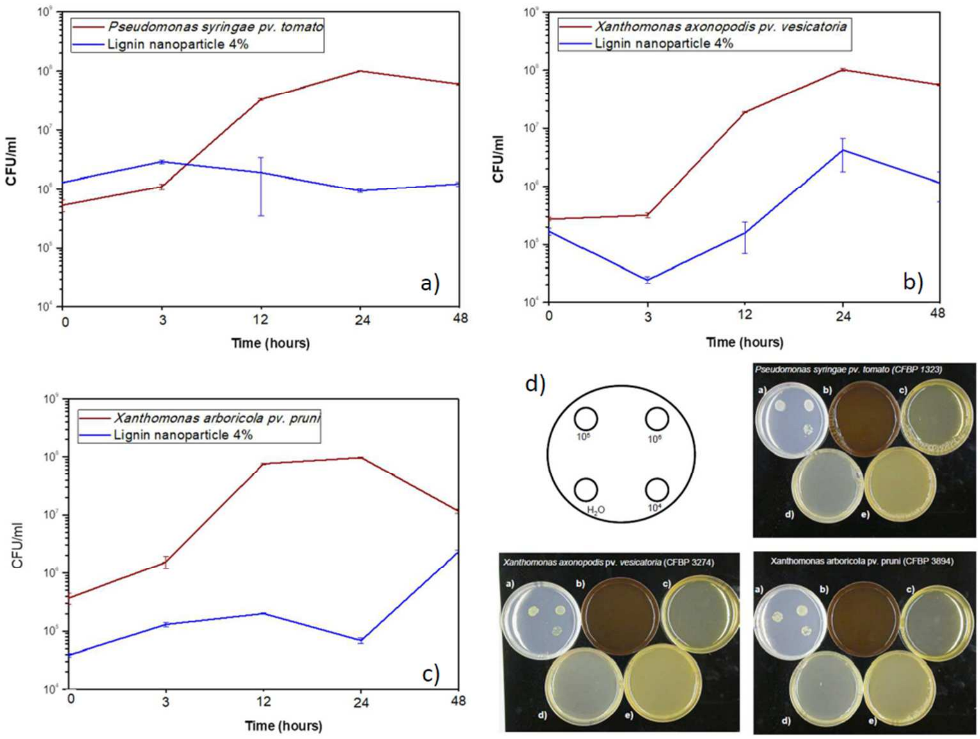

Figure 6: Bacterial growth in broth for Pseudomonas syringae pv. Tomato (a), Xanthomonas arboricola pv pruni (b) and Xanthomonas axonopodis pv. Vesicatoria (c); Assay incorporation of lignin nanoparticles for all bacterial strains (Pst, Xav and Xap), used at different concentrations (1x104 CFU/mL, 1x105 CFU/mL and 1x106 CFU/mL) for a) control; b) pristine lignin; c) LNP by H3PO4; d) LNP by H2SO4; e) LNP by HCL.

280x212mm (96 x 96 DPI)

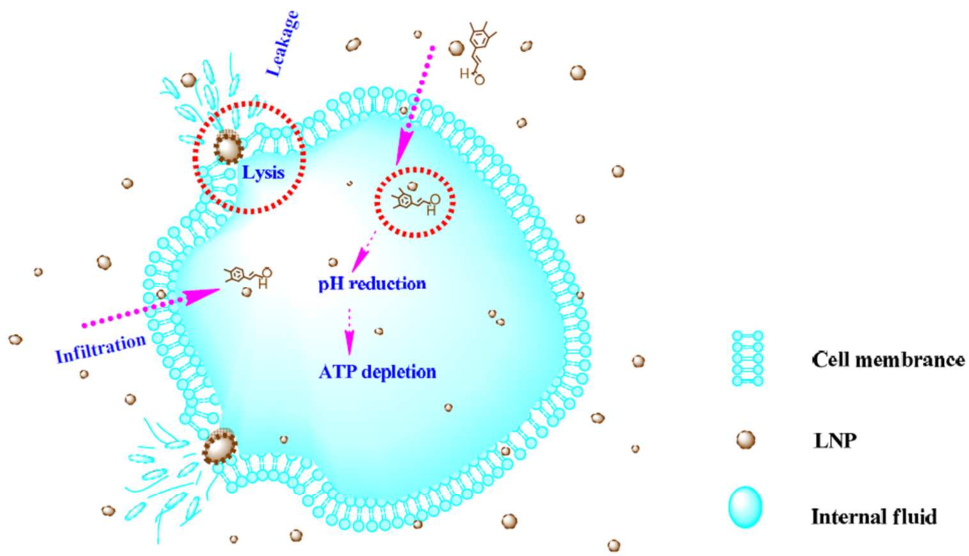

Figure 7: Involved mechanisms for antibacterial behavior of extracted LNP

262x162mm (96 x 96 DPI)

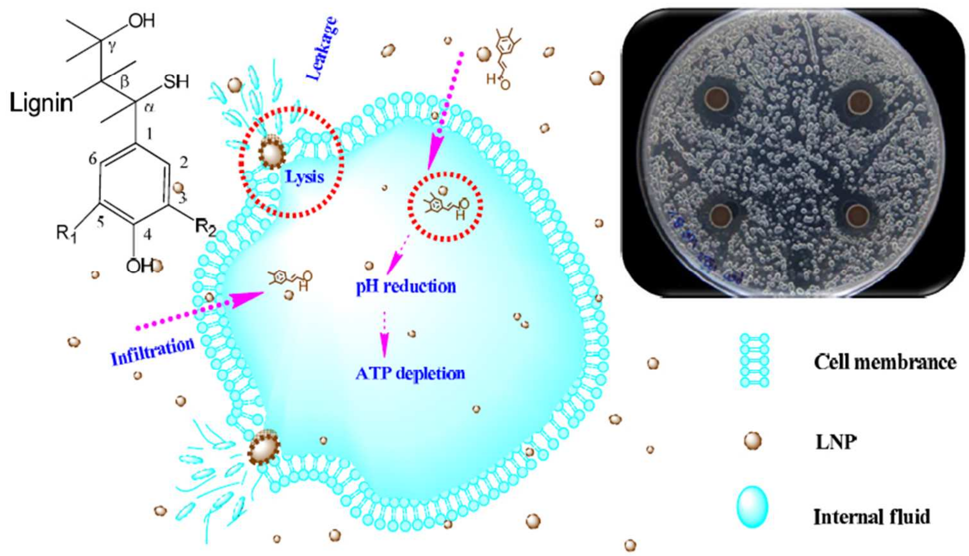

LNPs penetrate the cell wall by its lysis, react with ROS species inducing oxidative stress, ATP depletion and decrease of intracellular pH of plant bacteria.

232x137mm (96 x 96 DPI)